

A doubling of the Sun's coronal magnetic field during the past 100 years

M. Lockwood, R. Stamper & M. N. Wild

World Data Centre C-1 for STP, Rutherford Appleton Laboratory, Chilton, Didcot OX11 0QX, UK

The solar wind is an extended ionized gas of very high electrical conductivity, and therefore drags some magnetic flux out of the Sun to fill the heliosphere with a weak interplanetary magnetic field^{1,2}. Magnetic reconnection—the merging of oppositely directed magnetic fields—between the interplanetary field and the Earth's magnetic field allows energy from the solar wind to enter the near-Earth environment. The Sun's properties, such as its luminosity, are related to its magnetic field, although the connections are still not well understood^{3,4}. Moreover, changes in the

heliospheric magnetic field have been linked with changes in total cloud cover over the Earth, which may influence global climate⁵. Here we show that measurements of the near-Earth interplanetary magnetic field reveal that the total magnetic flux leaving the Sun has risen by a factor of 1.4 since 1964: surrogate measurements of the interplanetary magnetic field indicate that the increase since 1901 has been by a factor of 2.3. This increase may be related to chaotic changes in the dynamo that generates the solar magnetic field. We do not yet know quantitatively how such changes will influence the global environment.

The 'aa' index has been compiled from the range of variations in the geomagnetic field over periods of 3 hours, recorded since 1868 by pairs of near-antipodal magnetometers in England and Australia (see ref. 6 for a complete description of the index). Figure 1 demonstrates that the annual means <aa> show a marked variation with the sunspot cycle, but have also drifted upward throughout

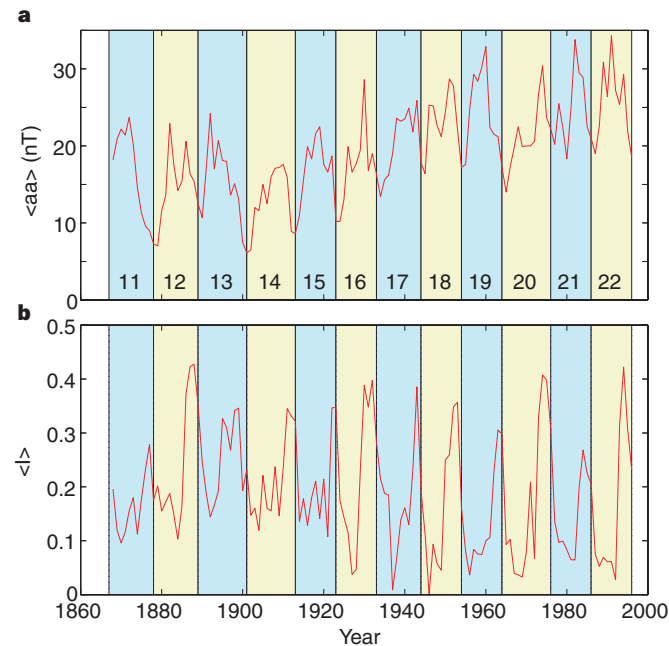


Figure 1 Annual means of **a**, the geomagnetic activity index, <aa>, and **b**, Sargent's recurrence index, <I>. I is defined for the jth 27-day Carrington rotation period as $I_j = (1/13) \sum_{k=-6}^{+6} C_{(j+k)}$, where C is the correlation coefficient between two consecutive 27-day intervals of 12-hourly aa values^{13,23}. The data are for 1868–1996, covering sunspot cycles 11–22: alternate solar cycles are shaded yellow and blue, starting at sunspot minima. Non-recurrent increases in aa are caused by solar disturbances, such as coronal mass ejections, hitting the Earth's magnetosphere. This occurs more frequently at sunspot maximum²⁵. In the declining phase of each sunspot cycle, <aa> is high because Earth intersects long-lived, fast solar-wind streams¹³. These emanate from coronal holes that have expanded to low heliospheric latitudes²² and rotate with the equatorial photosphere every 25 days. During this time, the Earth moves along its orbit, such that it intersects the same stream every 27 days giving recurrent geomagnetic storms and high <I> (ref. 13). Several long-term trends are apparent: for all phases of the solar cycle, <aa> increased gradually between 1900 and about 1955, before decreasing and then rising again during 1964–96. Similar trends can be seen in the sunspot number maxima (see Fig. 3). The recurrent element of geomagnetic activity at sunspot maximum, as quantified by <I>, fell during the early part of the century, but the sunspot minimum/declining phase peaks in <I> remained high with a tendency for greater values during even-numbered sunspot cycles²⁴.

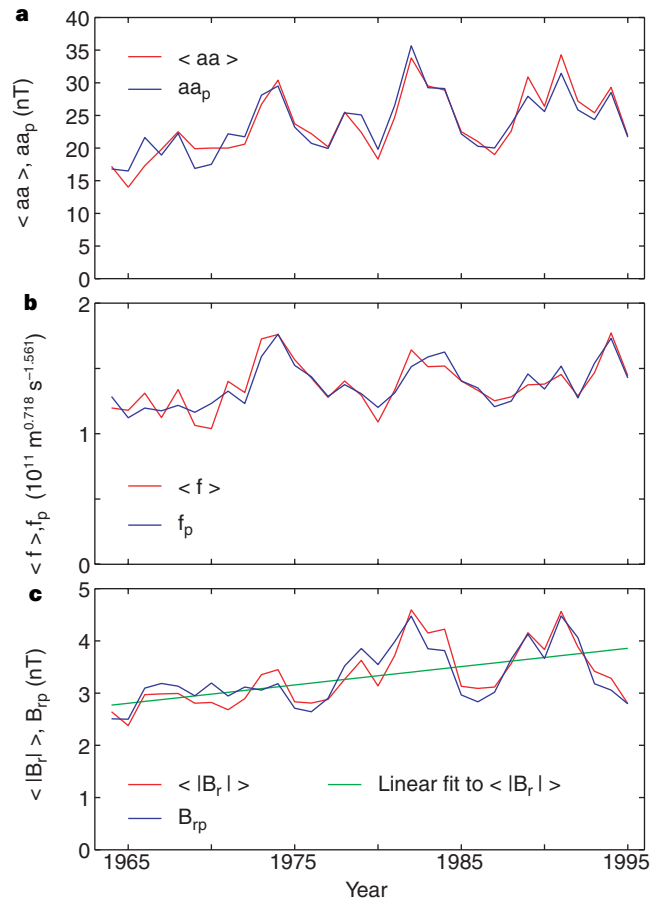


Figure 2 Time series of observed annual means and corresponding best-fit predicted values for 1964–96. **a**, Observed (<aa>) and predicted $aa_p = s_a P_a$ for the optimum coupling exponent α of 0.386 (ref. 7): a least-squares linear regression fit yields s_a , such that aa_p (in nT) = $(5.317 \times 10^{-17}) \{M_E \text{ in } T m^3\}^{2/3} \langle N_{sw} \text{ in } m^{-3} \rangle^{0.281} \langle v_{sw} \text{ in } km s^{-1} \rangle^{0.561} \langle B_{sw} \text{ in } nT \rangle^{0.772} (\sin^4(\theta/2))$. The correlation coefficient is 0.94, giving a significance level of $(100 - (1.3 \times 10^{-13}))\%$. There are larger uncertainties in the calibration of the interplanetary data, particularly N_{sw} before 1974: excluding these raises the correlation coefficient to 0.97, but lowers the significance level slightly to $(100 - (1.3 \times 10^{-11}))\%$. **b**, The annual means <f> = $\langle N_{sw} \text{ in } m^{-3} \rangle^{0.281} \langle v_{sw} \text{ in } km s^{-1} \rangle^{0.561} (\sin^4(\theta/2))$ and the best-fit predicted value, $f_p = s_f \langle I \rangle^\beta (aa)^\lambda + c_f$. The best-fit constants are $\beta = 0.263$, $\lambda = 1.303$, $s_f = 2.607 \times 10^4$ and $c_f = 1.893 \times 10^6$. The correlation coefficient is 0.91, for which the significance level is $(100 - (4.3 \times 10^{-11}))\%$. **c**, The annual means of the amplitude of the radial IMF component <|B_r|> and the predicted value $B_{rp} = s_B \langle B_{sw} \rangle$, where B_{sw} is the IMF magnitude. The least-squares fit gives the slope $s_B = 0.56$. The correlation coefficient is 0.92, for which the significance level is $(100 - (2.5 \times 10^{-12}))\%$. The green line in **c** is a linear regression fit to <|B_r|>.

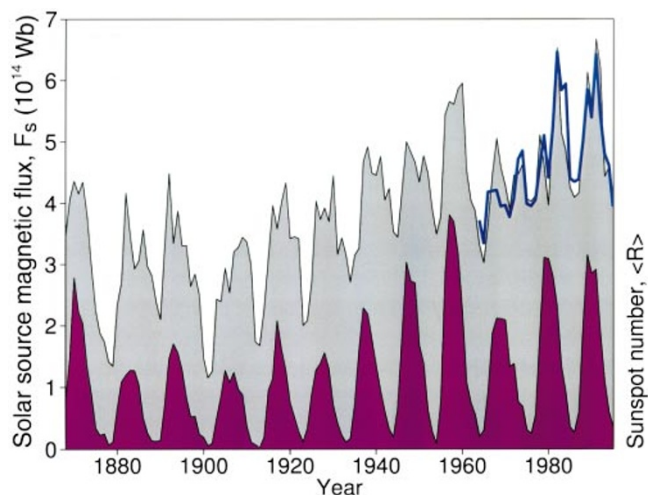


Figure 3 The total solar magnetic flux emanating through the coronal source sphere¹², F_s . Shown are the values derived from the geomagnetic aa data for 1888–1996 (black line bounding grey shading) and the values from the interplanetary observations for 1964–96 (thick blue line). The variation of the annual means of the sunspot number (R) is shown by the area shaded purple and varies between 0 and a peak of 190 for solar cycle 19.

most of this century. These changes are almost entirely due to variations in near-Earth interplanetary space⁷. Several attempts have been made to use the aa data to deduce the interplanetary and solar conditions before the ‘space age’^{8–10}. The success of these extrapolations depends critically on the quality of the correlation found between aa and the combination of the interplanetary parameters (the empirical ‘coupling function’¹¹) used to quantify the controlling influence of the solar wind and the interplanetary magnetic field (IMF). Recently, an unprecedentedly high and significant correlation coefficient of 0.97 has been obtained⁷.

We derive information on the magnetic field in the solar atmosphere (corona) from the (aa) data, using a procedure described in Methods. F_s is the magnetic flux that threads a roughly spherical ‘source’ surface in the corona where the Sun’s field becomes purely radial: it quantifies the amount of flux leaving the Sun and entering the heliosphere. The method employs three correlations of extremely high significance for the period 1964–96. Figure 2 shows the good agreement between observed yearly averages and their best-fit predicted values, derived using these correlations. Figure 2a shows the observed and predicted annual means of aa ($\langle aa \rangle$ and aa_p , respectively), Fig. 2b is the same for the function f (see Methods), and Fig. 2c is for the magnitude of the radial component of the IMF $|B_r|$.

The orientation of the IMF in annual averages is as predicted by the theory^{1,7} of the ‘Parker spiral’. This theory also predicts that the rise in the magnitude of the mean radial component (Fig. 2c) reflects a corresponding change in the coronal source field B_0 (equation (5)). A least-squares linear fit to $\langle |B_r| \rangle$ for 1964–96 (the green line in Fig. 2c) yields a percentage change (defined as 100 times the change, divided by the initial value) of 41% ($\pm 13\%$). In other words, there has been a rise by a factor of 1.41 over the last three solar cycles. This rise is present, but not commented on, in previously published coronal source field estimates, modelled from the measured solar photospheric field¹². Cosmic rays are shielded from the Earth by both the IMF and the solar-wind flow, and the observed decay in cosmic-ray fluxes (by 3.7% since 1964)^{7,13} is, at least qualitatively, consistent with the rise in the IMF.

The results of the extrapolation to before 1964 are shown in Fig. 3. The values of F_s derived from the aa data are shown in grey, and compare well with those from the observed annual means of the IMF radial component $\langle |B_r| \rangle$ for 1964–96 (thick blue line). The coronal source flux rises and falls in each solar cycle, lagging only

slightly behind the sunspot numbers R , shown in purple. The main differences between F_s and $\langle aa \rangle$ arise because the effects of the recurrent fast solar-wind streams (in the declining phase of each cycle¹³) have effectively been removed by our procedure. For data at all phases of the solar cycle, F_s has a correlation coefficient of 0.75 with the simultaneous R (giving a significance level of effectively 100%). To eliminate the solar-cycle variations, we have studied the 11-year running means and those for F_s and R vary in a very similar way. In 1901, the 11-year running mean of F_s was a minimum of 2.308×10^{14} Wb, but rose to a peak value of 5.325×10^{14} Wb in 1992. Thus in the intervening 91 years (covering roughly 8.5 sunspot cycles) there was a rise in the average solar source flux of 131% (that is, a rise by a factor of 2.31).

These changes in the solar magnetic field should be seen in the context of longer-term changes in the Sun, as inferred from historical sunspot and auroral observations¹⁴ and from the terrestrial abundances of isotopes such as ¹⁴C and ¹⁰Be (produced by cosmic-ray bombardment and deposited and stored, for example, in the polar icecaps)^{15,16}. The isotope data show that solar activity can largely disappear for periods of 50–100 years; one such period was the ‘Maunder minimum’ (circa 1645–1715), although there is evidence that during this interval a weak and cyclic magnetic field still emerged from the Sun¹⁶. By comparing the phase of the 88-year oscillation before and after the Maunder minimum, it has been inferred that the dynamo generating the solar field may be chaotic rather than quasi-periodic¹⁷: such behaviour may be relevant to the sudden changes in F_s around 1900 and 1960. Recent studies have linked changes in solar activity and aa with terrestrial climate change^{3–5,18}. The variation found here stresses the importance of understanding the connections between the Sun’s output and its magnetic field^{3,4} and between terrestrial global cloud cover, cosmic-ray fluxes and the heliospheric field⁵. □

Methods

We employ the optimum energy coupling function between the solar wind and the Earth’s magnetosphere derived by Stamper *et al.*⁷ using the dimensional analysis proposed by Vasyliunas *et al.*¹⁹. The solar-wind kinetic energy density dominates over the energy densities of both thermal motions and the IMF. This is incident on the geomagnetic field, which presents a roughly circular cross-section to the flow. A fraction of the incident energy is extracted, the power

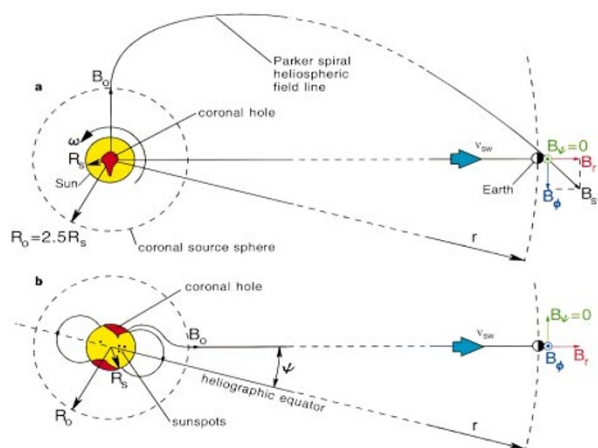


Figure 4 Schematic illustration of how the IMF B_{sw} emerges from holes in the solar atmosphere (coronal holes) and is dragged to Earth by the solar wind. The solar wind is flowing at v_{sw} radially away from the Sun in the heliosphere. The solar rotation winds the IMF into the Parker spiral¹. Such a field line is viewed here **a**, from north of the ecliptic plane and **b**, from a point in the ecliptic plane, to the dusk side of Earth. The coronal source surface is where the magnetic field, B_0 , is purely radial and is at a heliocentric distance of R_0 , which is roughly 2.5 times the solar radius, R_s (ref. 12). The magnetic flux threading this surface is F_s . The Ulysses spacecraft has shown that the radial component of the heliospheric field, B_r , is almost independent of the heliographic latitude ψ , (ref. 2).

transferred to the magnetosphere being⁷:

$$P_{\alpha} = \{k\pi/2\mu_0^{(1/3-\alpha)}\}M_E^{2/3}m_{sw}^{(2/3-\alpha)}N_{sw}^{(2/3-\alpha)}v_{sw}^{(7/3-2\alpha)}B_{sw}^{2\alpha}\sin^4(\theta/2) = aa_p/s_a \quad (1)$$

where m_{sw} is the mean ion mass, N_{sw} the concentration and v_{sw} the speed of the solar wind. B_{sw} is the IMF magnitude, θ is the IMF orientation ‘‘clock angle’’²⁰, M_E is the magnetic moment of the Earth (taken from the IGRF model²¹), s_a and k are constants and aa_p is the best-fit prediction of aa . From annual means for 1964–96, the best-fit ‘‘coupling exponent’’ α is found to be 0.386 (ref. 7), and s_a is obtained from a linear regression fit of $\langle aa \rangle$ against P_{α} . The largest factor contributing to the rise in $\langle aa \rangle$ since 1964 is an upward drift in B_{sw} with significant rises in N_{sw} and v_{sw} ; however the mean θ has grown somewhat less favourable for increasing $\langle aa \rangle$ (ref. 7). The dependence is sufficient to allow derivation of B_{sw} from $\langle aa \rangle$. In order to separate the effect of B_{sw} from that of the other interplanetary variables, we define a parameter f :

$$f = N_{sw}^{(2/3-\alpha)}v_{sw}^{(7/3-2\alpha)}\sin^4(\theta/2) \quad (2)$$

the variation of which is dominated by that in the solar wind speed v_{sw} . The annual mean of v_{sw} rises in the declining phase of solar cycles¹³ because the Earth repeatedly intersects fast solar-wind streams from low-latitude extensions of coronal holes²². These occur every 27 days and so also raise the geomagnetic recurrence index, I (see Fig. 1)²³. Hence we expect f and I to increase together in the declining phase of the sunspot cycle. However, I can remain high at sunspot minimum (whereas v_{sw} is lower) because aa values are low and relatively constant²⁴. Hence we adopted a relationship for a predicted f of the form:

$$f_p = s_f I^{\beta} aa^{\lambda} + c_f \quad (3)$$

where the exponents β and λ give the optimum correlation, and the constants s_f and c_f are then found from a linear regression fit. The primary justification for the use of equation (3) is that it yields a correlation which is comparable (in magnitude and significance) to the other two shown in Fig. 2. Note that f_p reproduces both the drift and 22-year cycle in f . From equations (1)–(3) we can obtain a formula for estimating B_{sw} from the aa index data series:

$$B_{sw} = \{[2aa\mu_0^{(1/3-\alpha)}]/\{s_a k \pi m_{sw}^{(2/3-\alpha)} M_E^{2/3} (s_f I^{\beta} aa^{\lambda} + c_f)\}\}^{1/(2\alpha)} \quad (4)$$

Parker spiral theory successfully predicts the radial and latitudinal variations of the annual means of the heliospheric field¹⁷:

$$B_{sw} = \{B_r^2 + B_{\phi}^2 + B_{\psi}^2\}^{1/2} = B_r \{1 + \tan^2 \gamma\}^{1/2} = B_0 (R_0/r)^2 \{1 + (\omega r \cos \psi / v_{sw})^2\}^{1/2} \quad (5)$$

where B_0 is the coronal source field at R_0 from the centre of the Sun¹², ω is the equatorial angular solar rotation velocity and ψ is the heliographic latitude (Fig. 4). In annual means, the modulus of the out-of-ecliptic IMF component $\langle |B_{\psi}| \rangle$ is well correlated with B_{sw} and the mean $\langle B_{\psi} \rangle$ is close to zero. The ‘garden hose angle’ γ of the IMF in the ecliptic plane (equal to $\tan^{-1} B_{\phi}/B_r$) remains close to 45°, and so the radial heliospheric field component B_r is roughly proportional to B_{sw} , that is, $B_r = s_B B_{sw}$ (Fig. 2c). In addition, recent observations by the Ulysses satellite have shown that latitudinal variations in the heliospheric field are small (B_r is independent of ψ)². This result has been used to derive the coronal source field B_0 from photospheric field measurements, and good agreement found with observations of B_r near the Earth at all phases of the solar cycle¹². The total magnetic flux of the sun that threads the source surface (radius R_0), F_s is:

$$F_s = (1/2)4\pi R_0^2 B_0 = 2\pi r^2 B_r = 2\pi r^2 s_B B_{sw} \quad (6)$$

where $r = 1$ AU for observations near Earth¹². The factor of one-half arises because half the field threading the source surface is inward, the other half outward. We can compute the solar flux F_s from the aa data using equations (4) and (6).

To extrapolate to before 1964, we assume that all three correlations (derived from the data for after 1964) were valid at all times since 1868. Specifically, we assume that the empirical functions $\sin^4(\theta/2)$ and f_p behave as they did after 1964. We also assume that the empirical coupling exponent α and the mean mass of the solar wind are constant, that Parker spiral theory applied, and that latitudinal variations in the heliospheric field were small then as now.

Received 21 December 1998; accepted 12 April 1999.

1. Gazis, P. R. Solar cycle variation of the heliosphere. *Rev. Geophys.* **34**, 379–402 (1996).
2. Balogh, A. et al. The heliospheric field over the south polar region of the sun. *Science* **268**, 1007–1010 (1995).

3. Willson, R. C. Total solar irradiance trend during cycles 21 and 22. *Science* **277**, 1963–1965 (1997).
4. Lean, J., Beer, J. & Bradley, R. Reconstruction of solar irradiance since 1610: implications for climate change. *Geophys. Res. Lett.* **22**, 3195–3198 (1995).
5. Svensmark, H. & Friis-Christensen, E. Variation of cosmic ray flux and global cloud coverage—a missing link in solar-climate relationships. *J. Atmos. Sol. Terr. Phys.* **59**, 1225–1232 (1997).
6. Mayaud, P. N. The aa indices: a 100-year series characterising the magnetic activity. *J. Geophys. Res.* **72**, 6870–6874 (1972).
7. Stamper, R., Lockwood, M., Wild, M. N. & Clark, T. D. G. Solar causes of the long-term increase in geomagnetic activity. *J. Geophys. Res.* (in press).
8. Russell, C. T. On the possibility of deducing interplanetary and solar parameters from geomagnetic records. *Sol. Phys.* **42**, 259–269 (1975).
9. Gringauz, K. I. in *Solar Wind 4* (ed. Rosenbauer, H.) (Rep. MPAE-W-100-81-31, MPI für Aeronomie, Lindau, Germany, 1981).
10. Feynman, J. & Crooker, N. U. The solar wind at the turn of the century. *Nature* **275**, 626–627 (1978).
11. Baker, D. in *Solar Wind-Magnetosphere Coupling* (eds Kamide, Y. & Slavin, J. A.) 17–38 (Terra Scientific, Tokyo, 1986).
12. Wang, Y.-M. & Sheeley, N. R. Jr Solar implications of Ulysses interplanetary field measurements. *Astrophys. J.* **447**, L143–L146 (1995).
13. Cliver, E. W., Boriakoff, V. & Bounar, K. H. The 22-year cycle of geomagnetic activity. *J. Geophys. Res.* **101**, 27091–27109 (1996).
14. Silverman, S. W. Secular variation of the aurora for the past 500 years. *Rev. Geophys.* **30**, 333–351 (1992).
15. Sonnet, C. P. Long-period solar terrestrial variability. *Rev. Geophys. (Suppl.: US Nat. Rep. to IUGG 1987–1990 909–914)* (1991).
16. Beer, J., Tobias, S. & Weiss, N. An active sun throughout the Maunder minimum. *Sol. Phys.* **181**, 237–249 (1998).
17. Feynman, J. & Gabriel, S. B. Period and phase of the 88-year solar cycle and the Maunder minimum: evidence for the chaotic sun. *Sol. Phys.* **127**, 393–403 (1990).
18. Cliver, E. W., Boriakoff, V. & Feynman, J. Solar variability and climate change: geomagnetic aa index and global surface temperature. *Geophys. Res. Lett.* **25**, 1035–1038 (1998).
19. Vasyliunas, V. M., Kan, J. R., Siscoe, G. L. & Akasofu, S.-I. Scaling relations governing magnetospheric energy transfer. *Planet Space Sci.* **30**, 359–365 (1982).
20. Scurry, L. & Russell, C. T. Proxy studies of energy transfer to the magnetosphere. *J. Geophys. Res.* **96**, 9541–9548 (1991).
21. Merrill, R. T., McElhinny, M. W. & McFadden, P. L. *The Magnetic Field of the Earth 34* (Academic, San Diego, 1996).
22. Wang, Y.-M., Hawley, S. H. & Sheeley, N. R. Jr The magnetic nature of coronal holes. *Science* **271**, 464–469 (1996).
23. Sargent, H. H. in *Solar Wind-Magnetosphere Coupling* (eds Kamide, Y. & Slavin, J. A.) 143–148 (Terra Scientific, Tokyo, 1986).
24. Hapgood, M. A. A double solar-cycle variation in the 27-day recurrence of geomagnetic activity. *Ann Geophys.* **11**, 248–253 (1993).
25. Webb, D. F. & Howard, R. A. The solar cycle variation of coronal mass ejections and solar wind mass flux. *J. Geophys. Res.* **99**, 4201–4220 (1994).

Acknowledgements. The data used are stored and made available via World Data Centre C1 for STP at RAL, which is funded by the UK Particle Physics and Astronomy Research Council and, until 1 April 1999, by the National Radio Propagation Programme of the Radiocommunications Agency. We also thank the many scientists who have contributed data to the WDC.

Correspondence and requests for materials should be addressed to M.L. (e-mail: m.lockwood@rl.ac.uk).

Origin of high critical currents in $\text{YBa}_2\text{Cu}_3\text{O}_{7-\delta}$ superconducting thin films

B. Dam*, J. M. Huijbregtse*, F. C. Klaassen*, R. C. F. van der Geest*, G. Doornbos*, J. H. Rector*, A. M. Testa†, S. Freisem§, J. C. Martinez||, B. Stäuble-Pümpin¶ & R. Griessen*

* *Institute COMPAS and Faculty of Sciences, Division of Physics and Astronomy, Vrije Universiteit, De Boelelaan 1081, NL-1081 HV Amsterdam, The Netherlands*

† *ICMAT, CNR, Area della Ricerca di Montelibretti, Rome, Italy*

§ *Kamerlingh Onnes Laboratory, Leiden University, PO Box 9506, NL-2300 RA Leiden, The Netherlands*

|| *Institut für Physik, Johannes Gutenberg Universität, D-55099 Mainz, Germany*

¶ *Department of Physics, Faculty of Science, Universidad Nacional de Colombia, Bogota, Colombia*

Thin films of the high-temperature superconductor $\text{YBa}_2\text{Cu}_3\text{O}_{7-\delta}$ exhibit both a large critical current (the superconducting current density generally lies between 10^{11} and 10^{12} A m⁻² at 4.2 K in zero magnetic field) and a decrease in such currents with magnetic field that point to the importance of strong vortex pinning along extended defects^{1,2}. But it has hitherto been unclear which types of defect—dislocations, grain boundaries, surface corrugations and anti-phase boundaries—are responsible. Here we make use of a sequential etching technique to address this question. We find that both edge and screw dislocations, which can be mapped